IEEE Open Journal of
Antennas and Propagation

Received 19 August 2022; revised 14 September 2022; accepted 19 September 2022. Date of publication 26 September 2022; date of current version 4 October 2022.

Digital Object Identifier 10.1109/OJAP.2022.3209522

Low-SAR Back Cover Mobile Antenna

HARRI VARHEENMAA, ANU LEHTOVUORI, PASI YLÄ-OIJALA, AND VILLE VIIKARI (Senior Member, IEEE)

Department of Electronics and Nanoengineering, Aalto University, 00076 Espoo, Finland

CORRESPONDING AUTHOR: H. VARHEENMAA (e-mail: harri.varheenmaa@aalto.fi)

This work was supported by the Aalto ELEC Doctoral School.

ABSTRACT A novel antenna design with a low specific absorption rate (SAR) is introduced. The antenna has a very low profile and it is designed to be placed on the back cover of a mobile device at around 2 GHz. The solution is based on nested loops which distribute the field over a large volume so that the maximum SAR value remains relatively low in the user's tissue. The proposed design also provides relatively good efficiency, considering the extremely low profile, and the close proximity of lossy human tissue and the phone's main body. The manufactured prototype exhibits almost 50 % lower maximum SAR than a patch antenna used as a reference.

INDEX TERMS Antenna, efficiency, lossy structure, mobile antenna, multiport antenna, specific absorption rate.

I. INTRODUCTION

THE REQUIREMENTS for antennas of modern mobile devices are constantly growing. Both the increasing number of antennas and the need for narrow bezel screens have reduced the available space for antennas. The metallic rim is fully occupied with a low-band (700–960 MHz) and other sub-6 GHz antennas. Currently, the millimeter wave arrays may also occupy space on the rim, and therefore, there is a need for realizing antennas in new locations.

One promising and yet rarely explored option is to place planar antennas on the back cover of the device [1]. The space between the back cover and the battery is typically only about 1 mm, which makes it challenging to achieve good efficiency. Another challenge is that the antenna radiates mainly towards the user when the phone is in the hand or inside the pocket. Consequently, the specific absorption rate (SAR), which measures absorbed power per unit mass of tissue, can exceed the allowed safety limits.

The easiest ways to decrease SAR are to lower the transmit power at the cost of reduced coverage or to place the antenna as far as possible from the user. These options, however, are rarely usable solutions for modern mobile devices. Other, more advanced techniques to reduce SAR include, for example, insulating the antenna with wave-absorbing material or shielding it [2], [3], [4], [5], [6], [7], [8]. The downside of these methods is that they tend to decrease the efficiency, bandwidth, and gain of the antenna [7]. Metamaterial structures have also been studied for SAR reduction [9], [10], [11]. These structures are not suitable solutions for back-cover antennas where the space is very limited.

This letter describes a novel back-cover antenna design that maximizes the ratio of total efficiency and SAR in cases where the antenna is used in close proximity to the human body. By using adequately shaped loops and slots on the antenna, the electromagnetic fields spread over a wider area than in conventional patch antennas with a solid patch. Consequently, significantly lower SAR can be obtained compared to the reference antenna with equally strong radiated fields. A design procedure and an operational principle of the proposed antenna are explained in detail. The performance of the proposed design is verified with measurements.

II. ANTENNA DESIGN

Back-cover mobile antennas require planar designs. The major challenge comes from the close proximity of the ground plane, which remarkably reduces the efficiency of the antenna [12], [13]. In addition, it would be beneficial to keep also other dimensions of the antenna small so that its placement would be easier, coupling to rim antennas would be smaller, and even several similar antennas could be used as multiple-input multiple-output antennas.

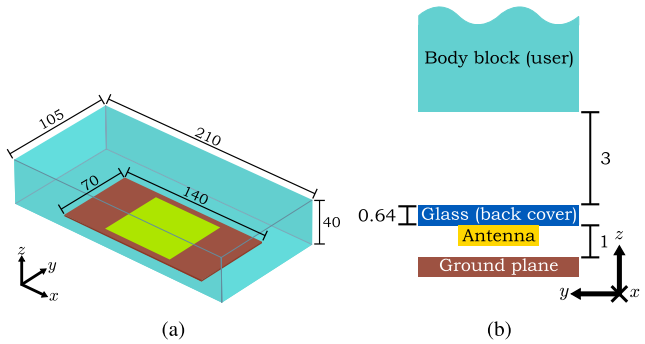

FIGURE 1. (a) Overview and (b) side view of simulation setup. In (a) the antenna locates at the yellow area and the top (glass) PCB is removed for better illustration. The metal thickness is enlarged in (b) for better visualisation. All dimensions are in mm.

A. SIMULATION MODEL

Fig. 1 illustrates the simulation model used in this paper. In this scenario, a mobile device is at a distance of 3 mm from the body, corresponding to the situation where the phone is placed inside of the breast pocket. The antenna is realized on the inner surface of the back cover of the phone. The battery and the frame of the phone is modelled as a 35 μm thick 140 mm$\times$70 mm copper ground plane. The distance between the antenna and the battery (ground plane) is only 1 mm.

The body phantom block is modelled with a 210 mm$\times$105 mm$\times$40 mm rectangular brick with parameters $\varepsilon_r = 39.56$, $\sigma = 1.52$ S/m, and $\rho = 1000$ kg/m^3 (at 1.9 GHz). These parameter values correspond to Speag Head Tissue Simulating Liquid (HBBL600-10000V6) [14] which is later used in the measurements.

The location of the antenna between the metallic ground plane and the body block decreases efficiency and requires the use of high input power. This easily leads to high SAR that can exceed the regulatory limits [15], [16]. However, attempts to solely minimize SAR easily decrease the total efficiency of the antenna. Therefore, we define a figure-of-merit (FoM) that takes into account this trade-off and describes the ratio of the total efficiency η_{tot} and the maximum SAR:

$$\text{FoM} = \xi \frac{\eta_{\text{tot}}}{\max(\text{SAR})}. \tag{1}$$

Here $\xi = P_{\text{in}}/m$, with input power P_{in} and mass m (either 1 g or 10 g depending on the used SAR standard), is a scaling factor to make FoM a unitless number. This enables the comparison of different antenna structures with different input powers.

SAR is related to the electric field intensity and the maximum SAR typically takes place close to the body surface [8]. We aim at wider (surface) SAR distribution to avoid high SAR peak values. This goal can be achieved by properly controlling the surface current distribution on the antenna.

Fig. 2 shows the design evolution of the antenna from the unbroken patch (a) to the final proposed design (f). While studying different antenna designs we found three facts that

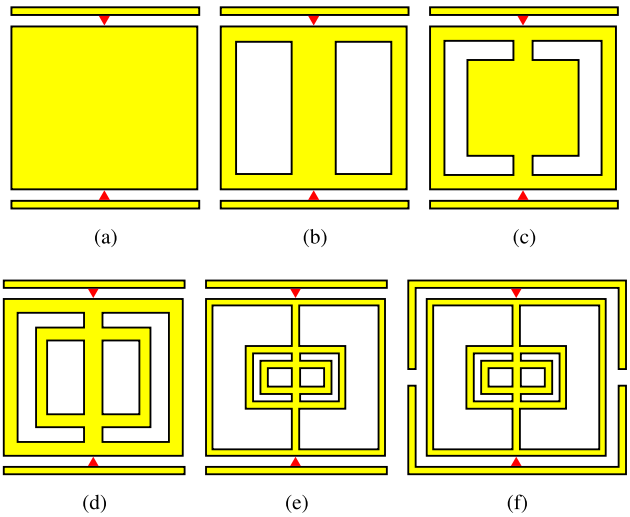

FIGURE 2. Antenna design evolution. Dimensions are not in scale.

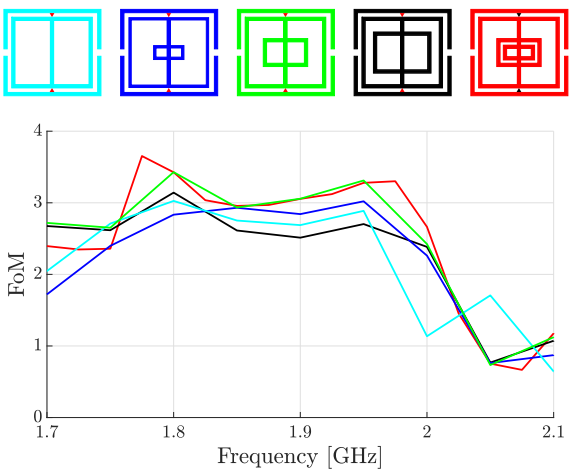

FIGURE 3. FoM with different numbers and sizes of the loops. The proposed design is the red one.

are important to achieve high FoM. Firstly, I-shaped slots (b) modify the current distribution and electric fields on the antenna. Thus, the SAR pattern spreads over a wider area, which reduces the maximum SAR. The surface currents distribute even more when slots are U-shaped, as in design (c).

Since the currents on the inner part of the patch concentrate on the edges, metal can be removed from the inner part of the patch so that it forms two nested loops, design (d). The second key part of the antenna is an unbroken metallic path (blue part in Fig. 4) between the feeding ports since without it antenna does not radiate properly. Fig. 3 illustrates FoM with different numbers and sizes of the loops while other dimensions are kept constant. FoM improves when a loop is added (blue) and FoM increases at the same time while the size of the loop grows, until after a certain point (black), it starts to decrease again. The additional loop inside the second one (red) distributes currents slightly more and therefore achieved FoM is a little better. The final proposed design (red) includes three nested loops (green part in Fig. 4).

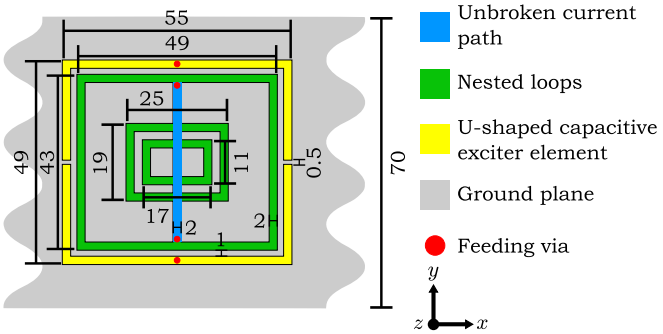

FIGURE 4. Dimensions (in mm, not in scale) of the proposed prototype antenna design. The antenna is placed on the top of the ground plane (grey) of dimensions 140 mm×70 mm (part of it is removed for better illustration). The antenna parts (made of copper) are marked with colour codes.

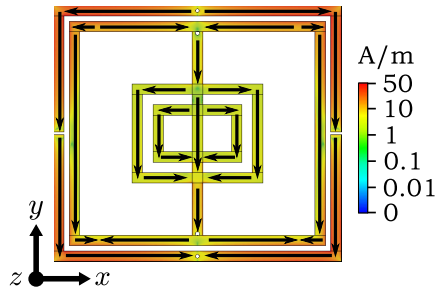

FIGURE 5. The real part of the surface current of the proposed design at 2 GHz. Colour indicates the amplitude of the current and arrows the direction.

The last key feature of the proposed antenna design is capacitive exciter elements. Arms are added to I-shaped (f) exciter elements to improve matching. Two equal U-shaped exciter elements (yellow part in Fig. 4) are placed close to the antenna (1 mm) to achieve good coupling between the exciter elements and the antenna. The best matching of the proposed design is obtained when the gap between the U-shaped capacitive exciter elements is small enough, about 1 mm. The feeding signals have equal amplitudes and opposite phases as in [17], [18], [19]. The final design and its dimensions are shown in Fig. 4. The different parts of the antenna are marked with colour codes.

The surface currents of the proposed antenna are analyzed in Fig. 5. The opposite phases of the feeding signals are needed to produce good radiation and then relatively strong currents can be seen in all parts of the design.

B. PROTOTYPE

Figs. 6(a) and 6(b) illustrate the manufactured antenna PCBs and Fig. 6(c) shows the power splitter PCB for the proposed design which is used to produce equal feeding signals and 180° phase difference. Fig. 7(a) shows simulated S-parameters of the power splitter. The equal amplitudes are executed so that the power splitter, which is based on a quarter-wave transformer, divides the power that is fed through an SMA connector equally to each branch. This is demonstrated in Fig. 7(a). The opposite phase is achieved by making a 180° line about half-wavelength longer than the

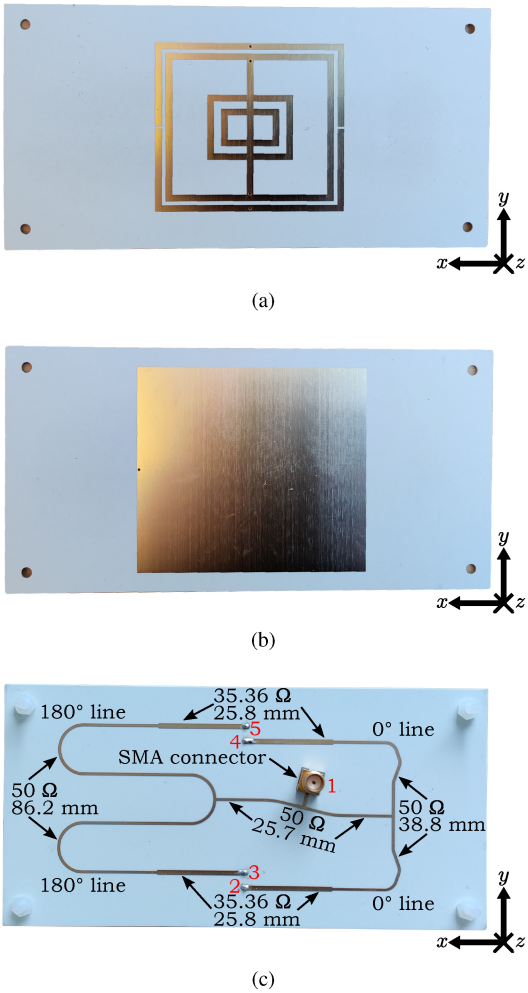

FIGURE 6. Manufactured designs: (a) proposed antenna PCB, (b) reference antenna PCB, and (c) power splitter PCB for the proposed antenna. The width of the 50 Ω line is 0.89 mm and the width of the 35.36 Ω line is 1.52 mm. The alignment nylon screws are in the corners. The port numbering of the power splitter is marked with red colour.

0° line. Figure 7(b) illustrates that the wanted 180° phase difference is achieved around 2 GHz.

Fig. 8 illustrates the exploded view of the proposed antenna prototype. This sandwich-like structure contains two printed circuit boards (PCB) and a 1 mm foam layer between them. The bottom PCB is made of 0.422-mm thick Rogers RO4350B ($\varepsilon_r = 3.66$, $\tan\delta = 0.0031$, and $\rho = 1.86\,\mathrm{g/cm^3}$). The bottom PCB includes the ground plane modelling the main body of the phone and the power splitter circuit on the opposite side. On top of that is 1-mm thick Rohacell 71 HF foam ($\varepsilon_r = 1.075$, $\tan\delta < 0.0002$, and $\rho = 75\,\mathrm{kg/m^3}$), which models the air gap between the main body of the phone (battery) and the back cover. The back cover glass with the antenna is modeled with 0.64-mm thick PCB, made of Rogers RO3006 ($\varepsilon_r = 6.5$, $\tan\delta = 0.0020$, and $\rho = 2.6\,\mathrm{g/cm^3}$) since its electrical properties are very close to that of the glass. The metal in both PCBs is 35 μm thick copper. All three layers are glued together and nylon screws are placed to each corner of the structure to keep the layers in

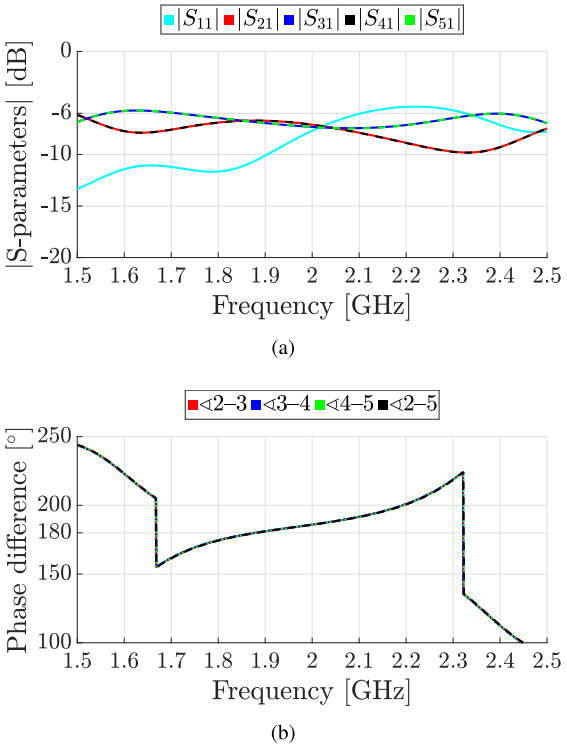

FIGURE 7. Simulated S-parameters (a) and phase differences (b) of the power splitter.

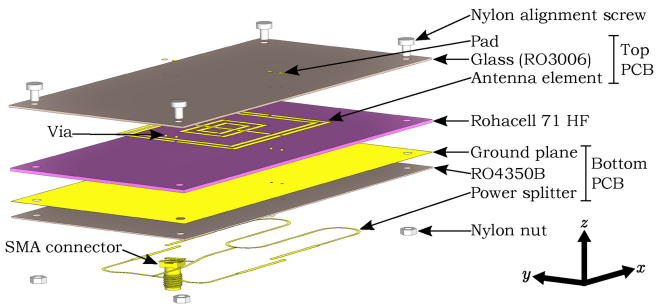

FIGURE 8. Exploded view of the proposed antenna.

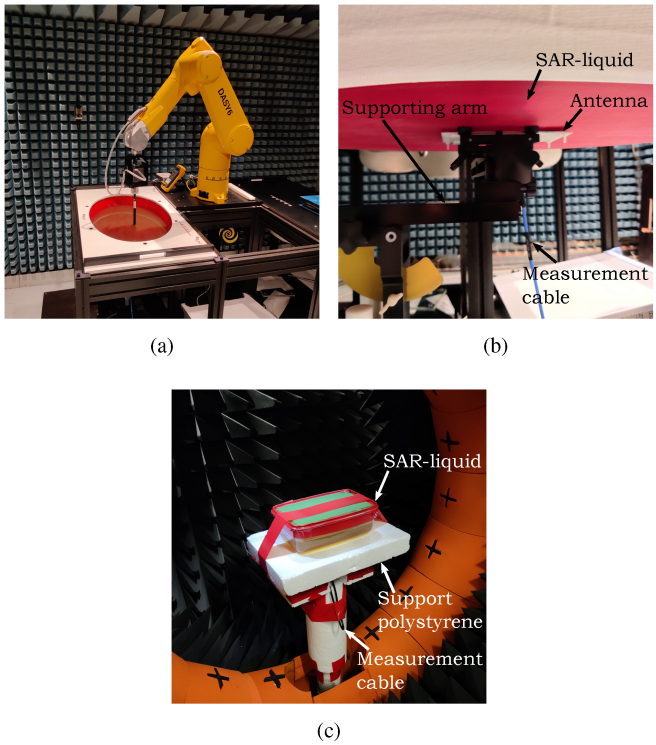

FIGURE 9. (a) Top view and (b) bottom view of the SAR measurement setup. (c) StarLab measurement setup.

place during the gluing. The antenna and the power splitter are connected and soldered together with a copper wire.

Also, the traditional rectangular patch antenna is manufactured for comparison. The size of the patch is 66 mm × 59 mm and it is fed at the center of the shorter edge. The reference patch antenna locates at the same place as the proposed one. Also, the reference antenna resonates at 2 GHz, but it is significantly larger covering about 30 % larger area than the proposed one. Since the reference antenna covers almost all available space in the *y*-axis direction, the possible other antennas on the rim would affect its operation more than the operation of the proposed design.

III. SIMULATION AND MEASUREMENT RESULTS

Both the proposed and the reference antenna designs are simulated with CST Studio Suite 2021. To verify the simulation results, SAR measurements are performed with Speag Dasy6 equipment, efficiency measurements are done with MVG StarLab 6-GHz system, and S-parameters are measured with a two-port Vector Network Analyzer (VNA). Fig. 9 illustrates SAR and StarLab measurement setups. In StarLab and S-parameters measurements, Fig. 9(c), the antenna is placed on supporting polystyrene foam, and 3-mm thick Rohacell foam is placed on top of that to model the air gap between the antenna and the body. The SAR liquid container is the uppermost layer in the measurement setup. The biggest difference between the SAR and StarLab setups is that in StarLab the liquid container lays on top of the antenna while in the SAR measurement setup the antenna is supported from below. The container does not compress the antenna and therefore the distance between the antenna and the liquid container is not the same.

The same Speag Head Tissue Simulating Liquid (shortly SAR-liquid) is used in both measurement setups but the size of the liquid container is different. The size of the liquid container and the amount of the liquid in StarLab measurements is the same as in the body model used in the simulations but in the SAR measurements, the container is much larger. This does not have any significant effect on the measurement results since maximum SAR is significant only close to the antenna.

Both the measured and simulated S-parameters for the proposed and reference antennas are shown in Fig. 10. The bandwidth of the reference antenna is larger whereas the operation of the proposed antenna is specifically optimized to the certain frequency. In both cases, the reference and

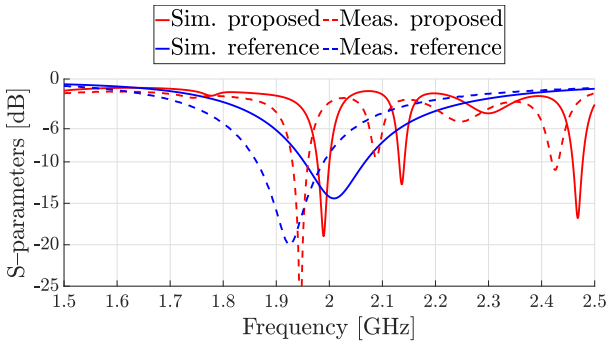

FIGURE 10. Simulated and measured S-parameters of the proposed and reference designs as functions of frequency.

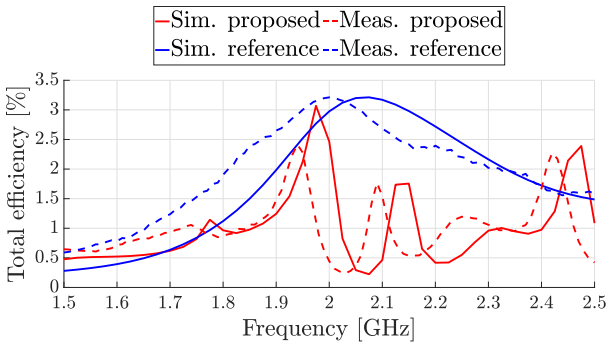

FIGURE 11. The simulated and measured total efficiency of the proposed and reference designs as functions of frequency.

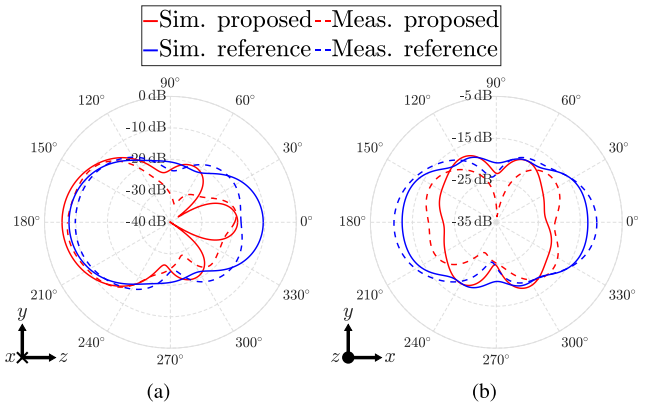

FIGURE 12. Measured and simulated realized gain of reference and proposed antennas at their resonance frequencies. (a) *yz* and (b) *xy* planes.

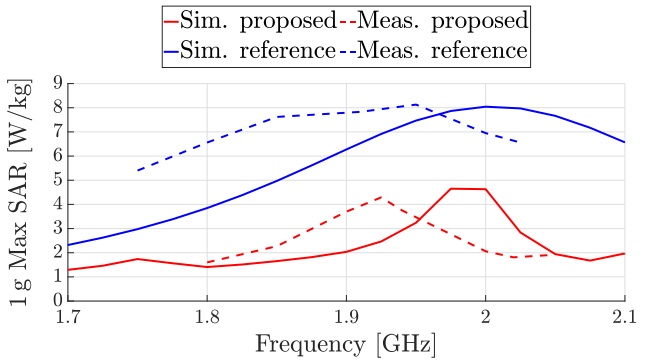

FIGURE 13. Simulated and measured maximum 1 g SAR of the proposed and references designs as functions of frequency. Input power in all cases is 27 dBm (0.5 W).

proposed antenna designs, the shapes of the measured and simulated S-parameter curves are very similar. However, the resonance frequencies have shifted a little, for the proposed antenna about 45 MHz and for the reference one about 80 MHz, due to small manufacturing inaccuracies.

Despite the smaller electrical size of the proposed design, the total efficiency of both the proposed and reference antennas are at the same level, as can be seen from Fig. 11. In both cases the efficiency is relatively low due to the close proximity of both the ground plane and a highly lossy body block. The same frequency shift between the measurements and simulations can be seen in both proposed and reference designs but again the overall shapes of the curves are similar. However, the measured maximum total efficiency of the proposed design is slightly lower than that of the simulated one. Fig. 12 shows measured and simulated realized gain of reference and proposed antennas at their resonance frequencies. Again, measured and simulated results are in line.

By comparing the maximum 1 g SAR values of the antennas, shown in Fig. 13, the benefit of the proposed design becomes evident. The input power used in both simulations and measurements is 27 dBm (0.5 W). At the resonance frequencies of the antennas, the maximum SAR value of the proposed antenna is less than half of that of the reference design. The shape of the measured and simulated SAR curves are similar but they have shifted a little. However, measured SAR has shifted about 25 MHz more to lower frequencies compared to the measured S-parameters and total efficiency. The reason for this is that the SAR and efficiency measurement setups are different, as explained in the previous section.

Figure 14 visualizes both the simulated and measured SAR patterns on the surface of the body block. With the reference antenna, the SAR pattern is highly concentrated in the center of the antenna, while the SAR pattern of the proposed design is distributed over a wider area and the maximum SAR takes place close to the sides of the antenna. In both cases, the measured and simulated SAR patterns are very similar.

Since SAR depends linearly on the used input power, the 1 g SAR safety limit (1.6 W/kg) can be attained by reducing the input power. The relative difference between the proposed and reference designs in SAR remains the same regardless of the input power. This is also verified by repeating the simulations with different input powers. The smaller relative SAR of the proposed design means that the proposed antenna can be used with 50 % higher input power than the reference antenna without exceeding the safety limits. Thus, it is possible to reach better coverage with the proposed antenna.

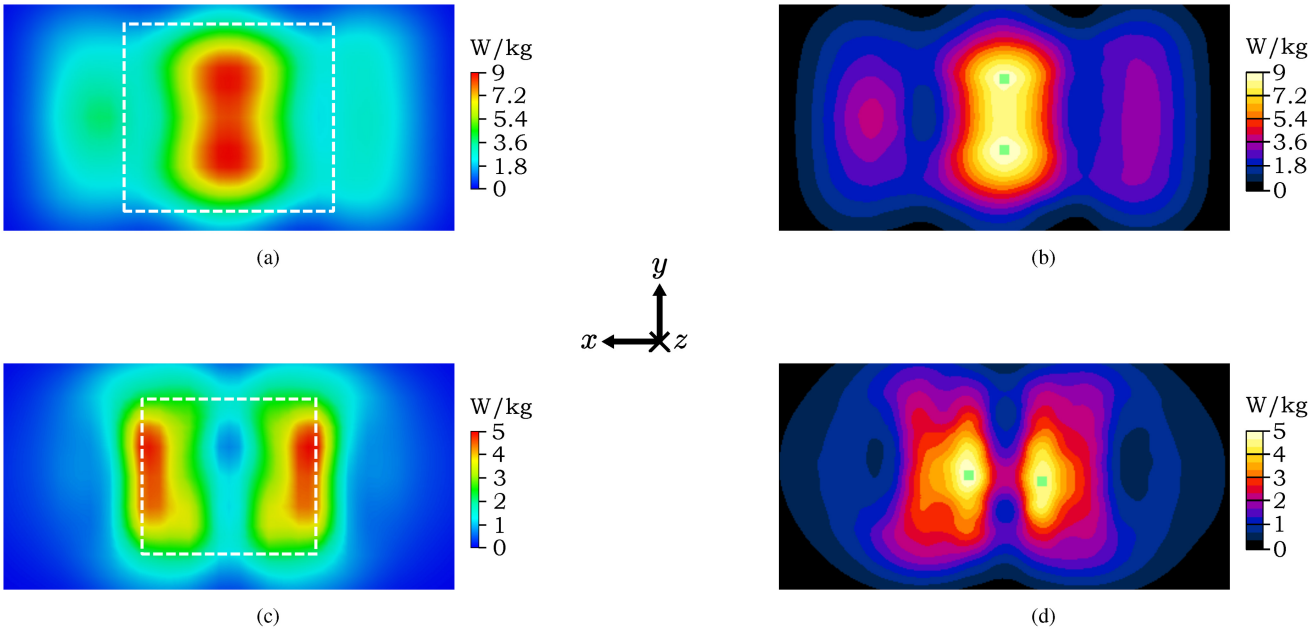

FIGURE 14. Simulated and measured SAR patterns on the surface of the body block. (a) Simulated reference design at 2.0 GHz, (b) measured reference design at 1.95 GHz, (c) simulated proposed design at 2.0 GHz, and (d) measured proposed design at 1.925 GHz. Input power in all cases is 27 dBm (0.5 W). The area where the antenna locates is plotted with a white dashed line.

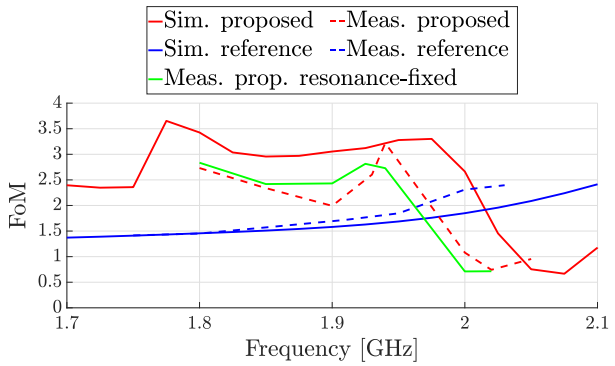

FIGURE 15. FoM based on simulations and measurements as a function of frequency. Input power in all cases is 27 dBm (0.5 W).

Figure 15 shows FoM computed using the simulated and measured results. The simulated FoM of the proposed design is about twice as high as in the reference case. For the reference antenna, the measurement and simulation-based FoMs are very similar, while for the proposed antenna the difference between the FoMs is bigger. This difference between the measured and simulated FoMs is a consequence of different measurement setups for SAR and total efficiency.

The green curve in Fig. 15 takes into account the frequency shift by changing the frequency points so that the resonance frequencies of SAR and total efficiency are the same. When this shift is taken into account, the difference between the measured and simulated FoMs of the proposed antenna becomes smaller. Regardless of the frequency shift in the measurement results, the proposed design gives better FoM than the reference one.

IV. CONCLUSION

This paper presented a novel low-SAR back-cover antenna having an ultra-low profile and producing a significantly higher total efficiency-maximum SAR ratio than a conventional patch antenna. The design is promising to be used in modern mobile devices where placing antennas to narrow gap between the main body and the back cover is challenging due to the SAR limits and poor total efficiency. The size of the proposed low-SAR antenna is remarkably smaller than that of the conventional rectangular patch antenna. This is an important benefit because a smaller size would allow easier placement of several antennas to the same device, e.g., to the metallic rim.

Measurements were performed to verify the simulations and they were well in line. The maximum SAR of the proposed design is almost 50 % lower than in the reference case. Decreased size and reduced maximum SAR of the proposed antenna give clear benefits when considering its applicability in practice.

ACKNOWLEDGMENT

The authors would like to thank Elmo Lepola for his help with simulations.

REFERENCES

[1] R. Luomaniemi, A. Lehtovuori, J. Ilvonen, A. Khripkov, and V. Viikari, "Extremely low-profile tunable multiport handset antenna," *IEEE Trans. Antennas Propag.*, vol. 70, no. 2, pp. 911–921, Feb. 2022.

[2] J. Ilvonen, R. Valkonen, J. Holopainen, O. Kivekäs, and P. Vainikainen, "Reducing the interaction between user and mobile terminal antenna based on antenna shielding," in *Proc. 6th Eur. Conf. Antennas Propag. (EUCAP)*, Mar. 2012, pp. 1889–1893.

[3] M. Jung and B. Lee, "SAR reduction for mobile phones based on analysis of EM absorbing material characteristics," in *IEEE Antennas Propag. Soc. Int. Symp. Dig. Held Conjunction USNC/CNC/URSI North Amer. Radio Sci. Meeting*, vol. 2, Jun. 2003, pp. 1017–1020.

[4] M. I. Kitra, C. J. Panagamuwa, P. McEvoy, J. C. Vardaxoglou, and J. R. James, "Low SAR ferrite handset antenna design," *IEEE Trans. Antennas Propag.*, vol. 55, no. 4, pp. 1155–1164, Apr. 2007.

[5] K. H. Chan, K. M. Chow, L. C. Fung, and S. W. Leung, "Effects of using conductive materials for SAR reduction in mobile phones," *Microw. Opt. Technol. Lett.*, vol. 44, no. 2, pp. 140–144, 2005. [Online]. Available: https://onlinelibrary.wiley.com/doi/abs/10.1002/mop.20569

[6] A. Hirata, T. Adachi, and T. Shiozawa, "Folded-loop antenna with a reflector for mobile handsets at 2.0 GHz," *Microw. Opt. Technol. Lett.*, vol. 40, no. 4, pp. 272–275, 2004. [Online]. Available: https://onlinelibrary.wiley.com/doi/abs/10.1002/mop.11350

[7] B. Lu, B. Pang, W. Hu, and W. Jiang, "Low-SAR antenna design and implementation for mobile phone applications," *IEEE Access*, vol. 9, pp. 96444–96452, 2021.

[8] H. H. Zhang, G. G. Yu, Y. Liu, Y. X. Fang, G. Shi, and S. Wang, "Design of low-SAR mobile phone antenna: Theory and applications," *IEEE Trans. Antennas Propag.*, vol. 69, no. 2, pp. 698–707, Feb. 2021.

[9] M. T. Islam, N. Misran, T. S. Ling, and M. R. I. Faruque, "Reduction of specific absorption rate (SAR) in the human head with materials and metamaterial," in *Proc. Int. Conf. Elect. Eng. Inform.*, vol. 2, Aug. 2009, pp. 707–710.

[10] R. Ikeuchi and A. Hirata, "Dipole antenna above EBG substrate for local SAR reduction," *IEEE Antennas Wireless Propag. Lett.*, vol. 10, pp. 904–906, 2011.

[11] J.-N. Hwang and F.-C. Chen, "Reduction of the peak SAR in the human head with metamaterials," *IEEE Trans. Antennas Propag.*, vol. 54, no. 12, pp. 3763–3770, Dec. 2006.

[12] D. Tayli and M. Gustafsson, "Physical bounds for antennas above a ground plane," *IEEE Antennas Wireless Propag. Lett.*, vol. 15, pp. 1281–1284, 2016.

[13] M. Gustafsson, M. Capek, and K. Schab, "Tradeoff between antenna efficiency and *Q*-factor," *IEEE Trans. Antennas Propag.*, vol. 67, no. 4, pp. 2482–2493, Apr. 2019.

[14] "Head tissue simulating liquids." SPEAG, Schmid & Partner Engineering AG. Accessed: Mar. 30, 2022. [Online]. Available: https://speag.swiss/components/materials-liquids/hsl/

[15] R. E. Fields, "Evaluating compliance with FCC guidelines for human exposure to radiofrequency electromagnetic fields," U.S. Federal Commun. Commission, Washington, DC, USA, document OET Bulletin 65, 1997. [Online]. Available: https://transition.fcc.gov/Bureaus/Engineering_Technology/Documents/bulletins/oet65/oet65c.pdf

[16] *IEEE Standard for Safety Levels With Respect to Human Exposure to Electric, Magnetic, and Electromagnetic Fields, 0 Hz to 300 GHz*, IEEE Standard C95.1-2019, Oct. 2019.

[17] Y. Kabiri, P. Gardner, and C. Constantinou, "Injection matched approach for wideband tunable electrically small antennas," *IET Microw. Antennas Propag.*, vol. 8, no. 11, pp. 878–886, 2014. [Online]. Available: https://ietresearch.onlinelibrary.wiley.com/doi/abs/10.1049/iet-map.2013.0700

[18] R. Luomaniemi, J.-M. Hannula, R. Kormilainen, A. Lehtovuori, and V. Viikari, "Unbroken metal rim MIMO antenna utilizing antenna clusters," *IEEE Antennas Wireless Propag. Lett.*, vol. 18, pp. 1071–1075, 2019.

[19] R. Kormilainen, J.-M. Hannula, T. O. Saarinen, A. Lehtovuori, and V. Viikari, "Realizing optimal current distributions for radiation efficiency in practical antennas," *IEEE Antennas Wireless Propag. Lett.*, vol. 19, pp. 731–735, 2020.